Fe 2 O 3 @BaTiO 3 Core–Shell Particles as Reactive Precursors for the Preparation of Multifunctional Composites Containing Different Magnetic Phases

ARTICLE *in* CHEMISTRY OF MATERIALS · AUGUST 2010

Impact Factor: 8.35 · DOI: 10.1021/cm1011982

9 AUTHORS, INCLUDING:

Vincenzo Buscaglia
Italian National Research Council
168 PUBLICATIONS **3,646** CITATIONS
SEE PROFILE

Lavinia-Petronela Curecheriu
Universitatea Alexandru Ioan Cuza
63 PUBLICATIONS **408** CITATIONS
SEE PROFILE

L. Mitoseriu
Universitatea Alexandru Ioan Cuza
178 PUBLICATIONS **2,387** CITATIONS
SEE PROFILE

4740 *Chem. Mater.* **2010,** *22,* 4740–4748
DOI:10.1021/cm1011982

CHEMISTRY OF MATERIALS
Article

Fe_2O_3@$BaTiO_3$ Core−Shell Particles as Reactive Precursors for the Preparation of Multifunctional Composites Containing Different Magnetic Phases

Maria Teresa Buscaglia,[†] Vincenzo Buscaglia,*[,†] Lavinia Curecheriu,[‡] Petronel Postolache,[‡] Liliana Mitoseriu,[‡] Adelina C. Ianculescu,[§] Bogdan S. Vasile,[§] Zhao Zhe,[#] and Paolo Nanni[†,○]

[†]*IENI-CNR, Via De Marini 6, I-16149 Genoa, Italy,* [‡]*Department of Physics, Alexandru Ioan Cuza University, Bulevardul Carol I, Nr. 11, Iasi 700506, Romania,* [§]*Department of Science & Engineering of Oxide Materials, Polytechnic University of Bucharest, 1-7 Gh. Polizu, P.O. Box 12-134, 011061 Bucharest, Romania,* [#]*Department of Materials and Environmental Chemistry, University of Stockholm, SE-10691, Stockholm, Sweden, and* [○]*Department of Process and Chemical Engineering, University of Genoa, Fiera del Mare, Pad. D, I-16129 Genoa, Italy*

Received April 28, 2010. Revised Manuscript Received June 22, 2010

Well-designed reactive precursors and templates allow for careful control of solid-state reactions at the nanoscale level, thus enabling the fabrication of materials with specific microstructures and properties. In this study, Fe_2O_3@$BaTiO_3$ core−shell particles have been used as precursors for the *in situ* fabrication of multifunctional composites containing a dielectric/ferroelectric phase and two magnetic phases with contrasting coercivities (Fe_2O_3/Fe_3O_4, $BaFe_{12}O_{19}/Ba_{12}Fe_{28}Ti_{15}O_{84}$). The formation of new magnetic phases occurs during sintering or post-annealing via reaction between $BaTiO_3$ and Fe_2O_3. The starting powders have been prepared using a multistep process that combines colloidal chemistry methods and a solid-state reaction. The nature and the amount of the magnetic phases and, consequently, the final magnetic properties of the composite can be controlled by varying the relative amount of Fe_2O_3 (30 or 50 vol %), the densification method (conventional or spark plasma sintering), and the processing temperature. The composites show constricted magnetic hysteresis loops with a coercivity of 0.1−2.5 kOe and a saturation magnetization of 5−16 emu/g. Composites obtained from powders containing 30 vol % Fe_2O_3 show, at temperatures of 20−80 °C and frequencies between 10 kHz and 1 MHz, a relative dielectric constant of 50 and dielectric losses of $< 10\%$.

1. Introduction

Ferroics are materials in which a characteristic property (polarization, magnetization, strain, etc.) can be switched between two stable states under a driving force or an external field. In multiferroics (MFs), at least two of the ferroic properties coexist in the same range of temperatures. Magnetoelectric (ME) MFs exhibit ferroelectricity and magnetic order (including ferromagnetism, antiferromagnetism, and ferrimagnetism) simultaneously. Possible applications are related to the coupling of electric and magnetic polarizations, and include multistate random access memories, transducers with magnetically modulated piezoelectricity, sensors for the measurements of magnetic/electric fields, modulation of transport properties, and capacitance by magnetic field.[1,2] Composite materials can be used to generate ME behavior from parent phases which themselves do not exhibit MF properties. This result can be achieved by means of mechanical coupling, combining magnetostrictive ($NiFe_2O_4$, $CoFe_2O_4$) and piezoelectric ($BaTiO_3$, $PbZr_xTi_{1-x}O_3$/PZT) compounds. An important advantage of the ME composites is that the ME coupling coefficient can be orders of magnitude higher than that of the best ME compounds.[1] The properties of ME composites can be tailored and designed by controlling the microstrucural features, such as the grain size and shape, the volume fraction, and the connectivity of the constituents.[3] Recent examples of composite architectures that provide optimal coupling are PZT-Terfenol and PZT-ferrite laminated composites,[4] in addition to heteroepitaxial structures composed of hexagonal arrays of $CoFe_2O_4$ nanopillars embedded in a $BaTiO_3$ matrix.[5]

*Author to whom correspondence should be addressed. E-mail: v.buscaglia@ge.ieni.cnr.it.

(1) Fiebig, M. *J. Phys. D: Appl. Phys.* **2005**, *38*, R123–R152.
(2) (a) Kim, H.; Islam, R. A.; Priya, S. *Appl. Phys. Lett.* **2007**, *90*, 012909. (b) Bergs, R.; Islam, R. A.; Vickers, M.; Stephanou, H.; Priya, S. *J. App. Phys.* **2007**, *101*, 024108. (c) Lou, J.; Reed, D.; Pettiford, C.; Liu, M.; Han, P.; Dong, S.; Sun, N. X. *Appl. Phys. Lett.* **2008**, *92*, 262502.
(3) Nan, C.-W. *Phys. Rev. B* **1994**, *50*, 6082.
(4) (a) Ryu, J.; Carazo, A.; Uchino, K.; Kim, H. E. *Jpn. J. Appl. Phys.* **2001**, *40*, 4948. (b) Cai, N.; Nan, C.; Zhai, J. Y.; Lin, Y. H. *Appl. Phys. Lett.* **2004**, *84*, 3516. (c) Srinivasan, G.; De Vreugd, C. P.; Flattery, C. S.; Laletsin, V. M.; Paddubnaya, N. *Appl. Phys. Lett.* **2004**, *85*, 2550.

Published on Web 07/29/2010

However, the low resistivity of the magnetic phase usually leads to high dielectric losses related to electrical conduction, Maxwell−Wagner interfacial polarization, and space-charge effects. These extrinsic effects may even dominate the final composite properties.[6] Since the piezoelectric component is far more insulating than the magnetic one, the above drawbacks can be partly overcome by preparing composites with core−shell grains consisting of a magnetic core and a piezoelectric shell. As a consequence, percolation of the more conductive phase can be avoided when the magnetic grains are completely isolated by the dielectric phase as realized in laminated composites. This possibility was not yet completely exploited, because, until now, only composite particles composed of a ferromagnetic/ferrimagnetic shell and a ferroelectric core were synthesized and characterized.[7]

A further approach to modify the properties of a multifunctional composite or even to add new functionalities is by introducing a third phase. However, the conventional mixing and sintering process offers only limited control on the final microstructure. In a more convenient way, additional phases can be introduced by *in situ* solid-state reactions between the constituents during the sintering process. The core−shell geometry looks quite promising for exploring this possibility, because the new phase will have a high contact area and a strong bonding with the parent phases and, consequently, a good coupling. Moreover, the final microstructure and phase composition will be completely controlled by the size of the cores and the thickness of the shell, thus resulting in materials with reproducible characteristics. In contrast, the use of powder mixtures will lead to less-predictable results, because the kinetics of solid-state reactions is strongly dependent on the particle size of parent oxides and mixture homogeneity. Likewise, it will be generally difficult to reproduce the final phase arrangement generated by the *in situ* solid-state reaction by just mixing all the given components and sintering.

An extensive investigation of the $BaO-TiO_2-Fe_2O_3$ system carried out by the group of T. Vanderah has revealed a rich crystal chemistry and the existence of at least 16 different quaternary compounds.[8] The oxides α-Fe_2O_3, Fe_3O_4, $BaFe_{12}O_{19}$, and $Ba_{12}Fe_{28}Ti_{15}O_{84}$ are very important, because of their magnetic properties. Fe_2O_3 hematite is a weak ferromagnet at room temperature, with a Curie temperature (T_C) of 950 K, a saturation magnetization (M_s) of the order of 0.2−0.4 emu/g, and a coercivity (H_c) of 1−4 kOe, depending on particle size.[9] Fe_3O_4 magnetite is a ferrimagnetic oxide with M_s = 90 emu/g, T_C = 858 K, and an H_c value on the order of 0.2 kOe.[10] Barium hexaferrite ($BaFe_{12}O_{19}$) has both high magnetization and large coercivity, with M_s = 70 emu/g, H_c = 4−6 kOe, and T_C = 723−743 K.[11] The magnetic properties of the quaternary layered ferrite $Ba_{12}Fe_{28}Ti_{15}O_{84}$ were reported only recently: M_s = 13 emu/g, H_c = 0.04 kOe, and $T_C \approx 700$ K.[12] Therefore, the $BaTiO_3-Fe_2O_3$ system was chosen as a model system for studying the in situ formation of composite materials containing a dielectric phase ($BaTiO_3$) and different magnetic phases.

In the present paper, we describe the synthesis of $Fe_2O_3@BaTiO_3$ particles, the formation of additional magnetic phases during sintering or post-annealing, and the magnetic and dielectric properties of the final composite materials.

2. Experimental Section

2.1. Preparation of $Fe_2O_3@BaTiO_3$ Particles. Hematite α-Fe_2O_3 particles with an average particle size of ~400 nm and narrow size distribution were prepared according to the method described by Sugimoto et al.[13] Shortly, 50 mL of a NaOH solution (5.4 mol/L) were added to 50 mL of a $FeCl_3$ solution (2 mol/L) at 75 °C under stirring. The resulting iron hydroxide gel was aged for 4 days at 100 °C. The final particles, after washing, were coated with a shell of amorphous hydrous titania obtained by hydrolysis of a solution of the peroxotitanium(IV) complex, using the same procedure reported in a previous paper.[14] The peroxotitanium complex was prepared by adding 5.42 mL of H_2O_2 (30%) to 100 mL of a solution obtained by dissolving 4.07 g $TiCl_4$ in water. The pH of this solution was increased to ~10 by adding 13.6 mL of aqueous ammonia (5.44 mol/L). Addition of 1g of Fe_2O_3 powder followed by slow heating to 95 °C and 5h aging at the same temperature, resulted in the formation of $Fe_2O_3@TiO_2$ core−shell particles. A suspension of 2.3 g of $BaCO_3$ nanoparticles (specific surface area = 28 m^2 g^{-1}, equivalent mean particle size = 55 nm) in 75 mL of a diluted ammonia solution at pH 8 was obtained at 95 °C by ultrasonication. This suspension was then slowly added to the suspension of the $Fe_2O_3@TiO_2$ particles while stirring. The carbonate nanoparticles preferentially adhere on the TiO_2 surface, resulting in a very good dispersion. The solid phase was finally separated, washed, and freeze-dried. Calcination for 4 h at 700 °C resulted in the reaction between the TiO_2 layer and the $BaCO_3$ nanoparticles with the formation of $Fe_2O_3@BaTiO_3$ nanocomposite particles (70 vol % $BaTiO_3$) with core−shell structure. Two different compositions, denoted as F1BT ($BaTiO_3$: 70 vol %−65 mol %−73 wt %) and F2BT ($BaTiO_3$: 50 vol %−44 mol %−53 wt %), were prepared.

(5) Zheng, H.; Wang, J.; Lofland, S. E.; Ma, Z.; Mohaddes-Ardabili, L.; Zhao, T.; Salamanca-Riba, L.; Shinde, S. R.; Ogale, S. B.; Bai, F.; Viehland, D.; Jia, Y.; Schlom, D. G.; Wutting, M.; Roytburd, A.; Ramesh, R. *Science* **2004**, *303*, 661.
(6) Mitoseriu, L.; Buscaglia, V. *Phase Trans.* **2006**, *79*, 1095.
(7) (a) Koo, Y. S.; Bonaedy, T.; Sung, K. D.; Jung, J. H.; Yoon, J. B.; Jo, Y. H.; Jung, M. H.; Lee, H. J.; Koo, T. Y.; Jeong, Y. H. *Appl. Phys. Lett.* **2007**, *91*, 212903. (b) Koo, Y. S.; Song, K. M.; Hur, N.; Jung, J. H.; Jang, T.-H.; Lee, H. J.; Koo, T. Y.; Yeong, Y. H.; Cho, J. H.; Jo, Y. H. *Appl. Phys. Lett.* **2009**, *94*, 032903.
(8) (a) Vanderah, T. A.; Loezos, J. M.; Roth, R. S. *J. Solid State Chem.* **1996**, *121*, 38. (b) Siegrist, T.; Vanderah, T. A. *Eur. J. Inorg. Chem.* **2003**, 1483.
(9) (a) Bødker, F.; Hansen, M. F.; Bender Koch, C.; Lefmann, K.; Mørup, S. *Phys. Rev. B* **2000**, *61*, 6826. (b) Sahu, K. K.; Rath, C.; Mishra, N. C.; Anand, S.; Das, R. P. *J. Colloid Interface Sci.* **1997**, *185*, 402.
(10) (a) Özdemir, Ö.; Dunlop, D. J. *Earth Planet. Sci. Lett.* **1999**, *165*, 229. (b) Adachi, T.; Wakiya, N.; Sakamoto, N.; Sakurai, O.; Shinozaki, K.; Suzuki, H. *J. Am. Ceram. Soc.* **2009**, *92*, S177.
(11) Nicolas, J. Microwave Ferrites. In *Ferromagnetic Materials*; Wohlfarth, E. P., Ed.; North-Holland: Amsterdam, 1987; Vol. *2*, pp 243−296.
(12) Frunza, R. C.; Ciuchi, I. V.; Curecheriu, L. P.; Postolache, P.; Mitoseriu, L.; Bassano, A.; Canu, G.; Buscaglia, V.; Ianculescu, A. C. Submitted to Scr. Mater.
(13) Sugimoto, T.; Wang, Y.; Itoh, H.; Muramatsu, A. *Colloids Surf. A* **1998**, *134*, 265.
(14) Buscaglia, M. T.; Buscaglia, V.; Alessio, R. *Chem. Mater.* **2007**, *19*, 711.

2.2. Preparation of Multifunctional Composites. The powders were consolidated using two different sintering methods: (i) cold isostatic pressing at 200 bar, followed by conventional sintering in air (1 h at 1050 or 1150 °C) without application of external pressure, and (ii) spark plasma sintering (SPS). For SPS, the powder with 70 vol % $BaTiO_3$ was loaded directly into a cylindrical graphite pressure die. The die was then placed inside a Dr. Sinter 2050 furnace (Sumitomo Coal Mining Co., Tokyo, Japan), and the system was evacuated. Two different samples were fabricated by heating at 200 °C/min and then sintering for 4 min at 1050 °C or for 3 min at 1100 °C. The heating was provided by a pulsed direct current flowing through the graphite die. During the entire heating and sintering process, a uniaxial constant pressure of 50 MPa was applied. The temperature was recorded by means of a pyrometer focused on a small hole in the graphite die wall. The pressure then was released, and the sample (a disk with diameter of 1.2 cm and thickness of 0.1−0.2 cm) was cooled at a rate of ~400 °C/min.

2.3. Characterization. Particle morphology and composite microstructure were investigated by scanning electron microscopy (SEM) (LEO 1450VP, LEO Electron Microscopy Ltd., Cambridge, U.K.), high-resolution scanning electron microscopy with a field emission gun (SEM-FEG) (Quanta Inspect F, FEI Co., The Netherlands), and high-resolution transmission electron microscopy (HRTEM) (Tecnai G^2 F30 S-TWIN, FEI Co., The Netherlands). The transmission electron microscopy (TEM) system was equipped with a STEM/HAADF detector and an energy-dispersive X-ray analysis (EDS) component to investigate the elemental composition and energy-filtered transmission electron microscopy−electron energy loss spectroscopy (EFTEM-EELS). Samples for HRTEM investigation were prepared according to standard procedures (cutting, grinding, and ion milling). Phase composition was determined by X-ray diffraction (XRD) (Philips PW1710, Co Kα radiation). The dielectric measurements were performed on electroded ceramics at 20−80 °C in the frequency range of 10^3−10^6 Hz with an impedance bridge (Agilent E4980A Precision LCR Meter). Magnetization-field hysteresis loops $M(H)$ were recorded at room temperature (RT) under magnetic fields (H) in the range of 0−14 kOe with a magnetometer (MicroMag VSM model 3900, Princeton Measurements Co.).

3. Results and Discussion

3.1. Microstructure and Phase Composition. The starting α-Fe_2O_3 particles (Figure 1a) have a predominant cubic morphology with rounded edges and a narrow size distribution (400−500 nm). The morphology of the $BaCO_3$−Fe_2O_3@TiO_2 powder mixture is shown in Figure 1b. The $BaCO_3$ nanocrystals are well-dispersed around the Fe_2O_3@TiO_2 particles. After calcination at 700 °C for 2 h, the reaction between $BaCO_3$ and TiO_2 is almost complete, and the XRD pattern of Figure 2 indicates only minor amounts of barium carbonate and $BaTi_2O_5$. Although a certain level of agglomeration was unavoidable, a well-defined particle morphology is still observed (Figures 1c and 1d). According to the literature, the formation of $BaTiO_3$ occurs by inward coupled diffusion of Ba^{2+} and O^{2-} ions from the $BaCO_3$/$BaTiO_3$ interface to the $BaTiO_3$/TiO_2 interface through the perovskite lattice.[15] Consequently the core−shell structure is preserved during the transformation from Fe_2O_3@TiO_2 to Fe_2O_3@$BaTiO_3$. As shown in Figure 3, the final particles are composed of a Fe_2O_3 core and a nanocrystalline $BaTiO_3$ shell composed of grains with 30−100 nm in size. The existence of the core−shell structure is well-supported by the results of EDS analysis (Figure 3). While Ba and Ti are predominant in the outer region, Fe is the main element in the central part. Formation of mixed Ba−Fe and Ba−Fe−Ti oxides was not revealed by XRD (Figure 2), meaning that the reaction between the Fe_2O_3 core and the $BaTiO_3$ shell is quite slow at 700 °C. In contrast, formation of the $BaFe_{12}O_{19}$ hexaferrite to a limited extent occurred after 2 h calcination at 800 °C (Figure 2). Similar results were obtained for the F2BT composition. $BaTiO_3$ is always present in its tetragonal ferroelectric modification, as indicated by the asymmetric broadening of the (200) reflection at 53.2° 2θ, in comparison to the (111) reflection at 45.7° 2θ. The broadening is related to the splitting of the (200) pseudo-cubic reflection into two peaks, (200) and (002), determined by the tetragonal strain of the unit cell. The phase composition of the composites is substantially

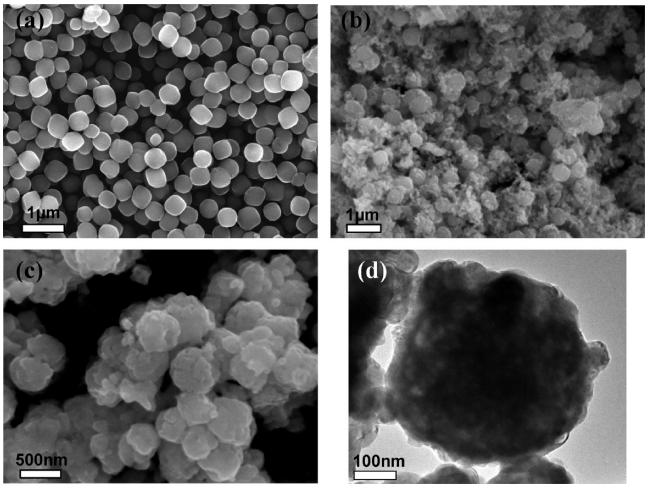

Figure 1. Morphology of (a) Fe_2O_3 particles (SEM-FEG), (b) $BaCO_3$−Fe_2O_3@TiO_2 mixture (SEM) (70 vol % $BaTiO_3$), and (c, d) Fe_2O_3@$BaTiO_3$ particles (70 vol % $BaTiO_3$) obtained by 2 h of calcination at 700 °C (the image in panel (c) obtained using SEM, and the image in panel (d) was obtained using TEM).

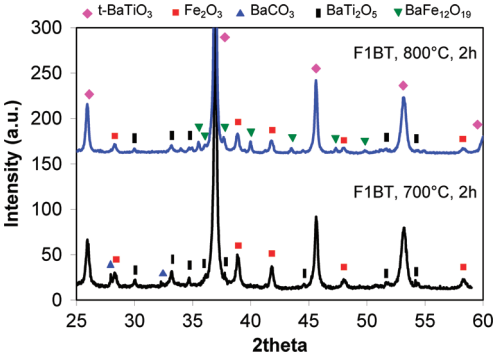

Figure 2. XRD patterns (Co Kα radiation) of Fe_2O_3@$BaTiO_3$ powders (70 vol % $BaTiO_3$) calcined at different temperatures. The patterns are normalized to the same maximum intensity.

(15) (a) Lotnyk, A.; Senz, S.; Hesse, D. *Solid State Ionics* **2006**, *177*, 429. (b) Lotnyk, A.; Senz, S.; Hesse, D. *Acta Mater.* **2007**, *55*, 2671. (c) Buscaglia, M. T.; Harnagea, C.; Dapiaggi, M.; Buscaglia, V.; Pignolet, A.; Nanni, P. *Chem. Mater.* **2009**, *21*, 5058.

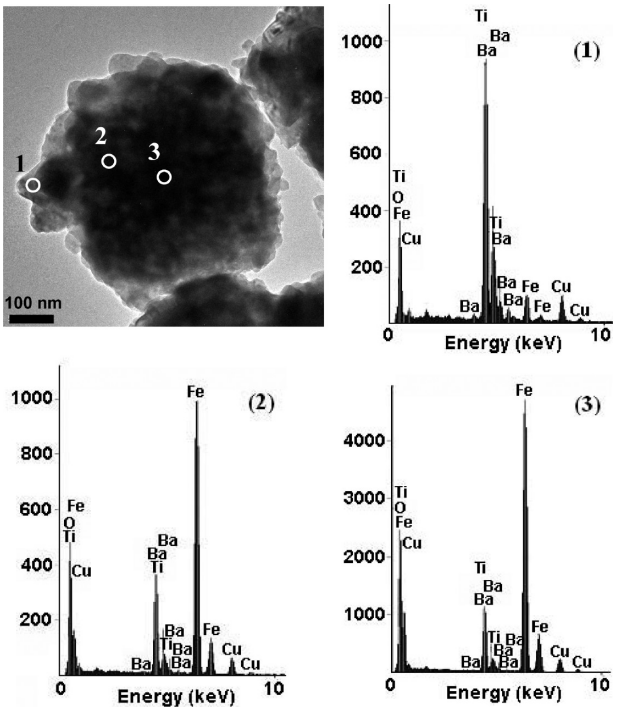

Figure 3. Morphology (TEM) and EDS spectra of a typical Fe_2O_3@$BaTiO_3$ particle (70 vol % $BaTiO_3$).

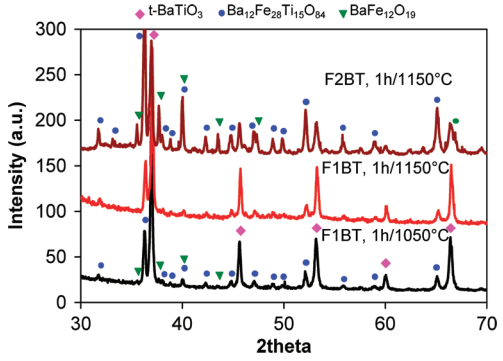

Figure 4. XRD patterns (Co Kα radiation) of composites fabricated from Fe_2O_3@$BaTiO_3$ core−shell particles by conventional sintering. The patterns are normalized to the same maximum intensity.

different from that of the original Fe_2O_3@$BaTiO_3$ particles. The XRD pattern of the composite fabricated from the F1BT powder by sintering at 1050 °C (Figure 4) shows two new phases that were formed at the expense of Fe_2O_3: the quaternary ferrite $Ba_{12}Fe_{28}Ti_{15}O_{84}$ and a minor amount of the barium hexaferrite ($BaFe_{12}O_{19}$). After sintering at 1150 °C, the reaction between $BaTiO_3$ and Fe_2O_3 resulted in the formation of the $Ba_{12}Fe_{28}Ti_{15}O_{84}$ phase alone, at least within the detection limit of XRD (1−2 wt %). Assuming the complete transformation of hematite, the final composition should roughly correspond to ~30 vol % $BaTiO_3$ and ~70 vol % $Ba_{12}Fe_{28}Ti_{15}O_{84}$. However, the overall stoichiometry of the powder requires also the formation of a third phase, unless the Ti imbalance is accommodated by formation of non-stoichiometric phases. Additional compounds were not observed by XRD, because they are either present in a small amount or the corresponding peaks strongly overlap

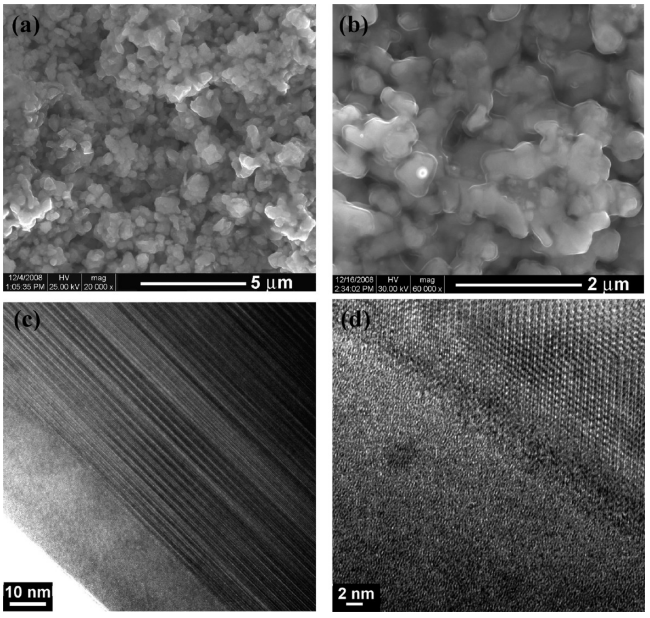

Figure 5. Microstructure of composites fabricated from Fe_2O_3@$BaTiO_3$ core−shell particles by conventional sintering (1 h at 1050 °C): (a) F1BT, SEM-FEG (fracture surface); (b) F2BT, SEM-FEG (fracture surface); (c,d) F2BT, HRTEM.

with those of the main phases. Composites fabricated from the F2BT powder show a similar phase composition (Figure 4). The amount of quaternary ferrite increases whereas the amount of residual $BaTiO_3$ decreases, in comparison to the F1BT composite, because of the larger quantity of Fe_2O_3 contained in the starting powder. The barium ferrite is clearly observed even after sintering at 1150 °C. The microstructure of both the F1BT and F2BT composites corresponds to porous ceramics (10%−15% porosity) with grains of 300−600 nm (Figures 5a and 5b). The formation of elongated grains (Figure 5b) indicates a substantial microstructure modification in the F2BT compound induced by the reaction between $BaTiO_3$ and Fe_2O_3 with the formation of $BaFe_{12}O_{19}$ and $Ba_{12}Fe_{28}Ti_{15}O_{84}$. Surprisingly enough, the grains appear to be coated with a glassy phase. The glassy phase is particularly evident in the F2BT composites (see Figures 5b−d), where it forms a continuous film 20−30 nm thick on the surface of the underlying phase. The two phases are separated by a thin (3−5 nm) interdiffusion region (Figure 5d). According to EDS analysis, the amorphous phase is composed of Ba, Fe, Ti, and O, whereas other foreign elements were not revealed. Its composition (8.92 at. % Ba, 11.86 at. % Ti, and 24.29 at. % Fe) is enriched in Ti and Fe, in comparison to that of the quaternary ferrite (8.63 at. % Ba, 10.79 at. % Ti, and 20.14 at. % Fe). Analyses carried out in the inner crystalline region of Figure 5c gave the following composition: 3.26 at.% Ba, 6.16 at.% Ti, and 32.01 at.% Fe. Taking into account the XRD results, this iron-rich composition roughly corresponds to the $BaTi_xFe_{12-(4/3)x}O_{19}$ solid solution with $x = 2$. The formation of the surface glassy layer may be attributed to the existence of an eutectic melt,although no liquid phases are reported on the only available isothermal section (1200 °C) of the phase diagram.[8]

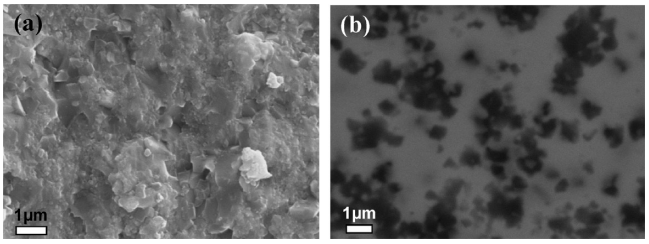

Figure 6. SEM images of the microstructure of a composite (70 vol % $BaTiO_3$) fabricated from Fe_2O_3@$BaTiO_3$ core−shell particles by SPS (4 min at 1050 °C): (a) fracture surface and (b) polished cross-section (backscattered electrons).

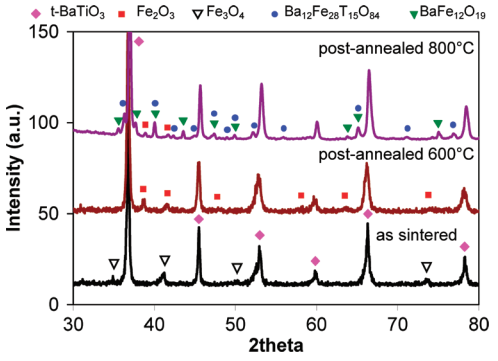

Figure 7. XRD patterns (Co Kα radiation) of composites fabricated from Fe_2O_3@$BaTiO_3$ core−shell particles by SPS (4 min at 1050 °C) and post-annealed in air at different temperatures. The patterns are normalized to the same maximum intensity.

F1BT composites fabricated by SPS were very dense, with a relative density of 98.4% after sintering at 1050 °C, and 99.4% after sintering at 1100 °C. The samples were very fragile and the extensive presence of cracks hampered the measurement of dielectric properties. The surface fracture shows Fe_2O_3 faceted grains or groups of grains embedded in a matrix of nanocrystalline $BaTiO_3$ composed of grains of 50−150 nm (Figure 6a). Isolated or grouped squared grains of Fe_2O_3 ~500 nm in size are clearly observed on the polished cross-section of Figure 6b. The hematite grains are generally well-separated by the perovskite phase, avoiding the percolation of the magnetic phase. The XRD pattern of the as-sintered SPS composite (Figure 7) shows the presence of tetragonal $BaTiO_3$ and magnetite Fe_3O_4. The formation of the spinel phase can be explained by the reduction of the Fe_2O_3 hematite particles induced by the graphite die and the absence of air during sintering. Annealing of the composite at 600 °C for 2 h in air leads to the oxidation of Fe_3O_4 to Fe_2O_3 hematite. Successive annealing in air for 2 h at higher temperatures (800 and 1000 °C) determines the formation of roughly comparable amounts of $BaFe_{12}O_{19}$ and $Ba_{12}Fe_{28}Ti_{15}O_{84}$, as shown in Figure 7. This in contrary to that observed for composites obtained by conventional sintering in air, for which the barium hexaferrite was always a minor phase (compare Figures 7 and 4). A significant amount of Fe_2O_3 was still detected after annealing at 800 °C and, thus, three ferromagnetic/ferrimagnetic phases coexist in the same material. After annealing at 1000 °C, hematite disappears and the relative intensities of the other two magnetic phases increase.

The results discussed above indicate that the final phase composition of composites obtained from Fe_2O_3@$BaTiO_3$ particles depends on three main factors: (i) the initial $Fe_2O_3/BaTiO_3$ volume ratio in the precursor core−shell particles, (ii) the sintering method (conventional or SPS), and (iii) the post-annealing temperature (in the case of the spark-plasma-sintered (SPSed) samples). According to the available phase diagram,[8] the equilibrium composition for both composites should correspond to a mixture of barium hexaferrite solid solution ($BaFe_{12-(4/3)x}Ti_xO_{19}$), layered ferrite $Ba_{12}Fe_{29}Ti_{15}O_{84}$, and $Ba_8Fe_{10}Ti_8O_{39}$ compound (the "K" phase described in ref 8). However, this latter phase was not observed (at least within the XRD detection limit), whereas tetragonal $BaTiO_3$ is always detected in substantial amounts. This means that the composites are not in thermodynamic equilibrium after the different thermal treatments. Since $BaFe_{12}O_{19}$ and $Ba_{12}Fe_{28}Ti_{15}O_{84}$ are both ferrimagnetic, their coexistence in the same material (see Figures 4 and 7) is expected to give rise to peculiar magnetic properties, as will be discussed in detail in section 3.2. The initial $Fe_2O_3/BaTiO_3$ volume ratio has a strong influence on the final phase composition, because the relative amount of the magnetic phases originated during sintering increases (see Figure 4) as the Fe_2O_3 fraction increases from 30 vol % (F1BT) to 50 vol % (F2BT). The coexistence of two magnetic phases, Fe_2O_3 and $BaFe_{12}O_{19}$, also occurs in the powders that have been calcined at 800 °C (see Figure 2). The densification of composites by SPS offers the opportunity to fabricate materials that contain an additional magnetic phase: Fe_3O_4. Because of the local reducing conditions that exist in the graphite die, Fe_2O_3 loses oxygen and transforms to the spinel phase. Quite likely, the transformation does not involve the entire sample volume but only the outer region, because of the short sintering time (3−4 min) and the high density of the material. A rapid reduction process is possible as long as the porosity is open (a relative density of $<93\%$). When the porosity is closed, reduction can only proceeds by solid-state reaction and the reaction kinetics will slow dramatically. Post-annealing in air at 600 °C produces reoxidation of Fe_3O_4 to Fe_2O_3 (see Figure 7). The formation of $BaFe_{12}O_{19}$ and $Ba_{12}Fe_{28}Ti_{15}O_{84}$ is observed after thermal treatment of the SPSed samples at 800 and 1000 °C. A quite unique situation is encountered after annealing at 800 °C, when three ferromagnetic/ferromagnetic phases coexist together, because the Fe_2O_3 cores are not yet completely consumed by the reaction with $BaTiO_3$.

Previous attempts to make use of the core−shell geometry in multiferroic composites were limited to particles composed of a ferroelectric core ($BaTiO_3$ or $Ba_{1-x}Sr_xTiO_3$) and a magnetic shell (γ-Fe_2O_3 or Fe_3O_4).[7,16,17] Koo et al.[7] coated $BaTiO_3$ particles ~100 nm in diameter with γ-Fe_2O_3 nanoparticles by means of a sonochemical method. Annealing of the resulting core−shell particles at 600 °C

(16) Mornet, S.; Elissalde, C.; Bidault, O.; Weill, F.; Sellier, E.; Nguyen, O.; Maglione, M. *Chem. Mater.* **2007**, *19*, 987.
(17) Park, H. K.; Choi, S. H.; Oh, J. H.; Ko, T. *Phys. Status Solidi B* **2004**, *241*, 1693.

in flowing N_2/H_2 atmosphere resulted in the formation of Fe_3O_4@$BaTiO_3$ structures. In an elegant investigation, Mornet et al.[16] decorated the surface of ferroelectric grains with superparamagnetic γ-Fe_2O_3 nanoparticles using a colloidal chemistry approach. Both types of particles were encapsulated with a thin silica shell. Mixed Fe_3O_4−$BaTiO_3$ powders were obtained by Adachi et al.[10b] using spray pyrolysis. In any case, because the thermal treatments were performed at relatively low temperatures, the formation of additional magnetic phases was not observed and the magnetic properties, taking into account the dilution effect due to the ferroelectric phase, were similar to those of the pure magnetic phase. Fe_3O_4-encapsulated $BaTiO_3$ particles were also prepared by Park et al.,[17] again using sonochemistry, and the resulting powders were sintered at 900−1050 °C. Formation of a new phase was detected above 900 °C, but the authors were unable to identify it as the quaternary ferrite $Ba_{12}Fe_{28}Ti_{15}O_{84}$ and the magnetic hysteresis loops were not reported.

3.2. Magnetic Properties. The $M(H)$ hysteresis loops measured at RT on some selected powders and composites are shown in Figure 8. The values of the saturation magnetization (M_s), remnant magnetization (M_r), and coercivity (H_c) are reported for each material. All composites show a good saturation of magnetization, whereas the hysteresis loops of the powders calcined at 700 °C (see Figures 8a and 8d) are not well-saturated, because of the very broad distribution of the coercivity. The strong sensitivity of the magnetic properties to the initial powder composition and the thermal treatment is quite evident. The $M(H)$ loop measured for the F1BT powder annealed at 700 °C (Figure 8a) is consistent with the magnetic properties of α-Fe_2O_3. The saturation magnetization (0.08 emu/g) is comparable to that of bulk hematite (0.4 emu/g) if the fractional amount of magnetic phase (27 wt %) is considered. The coercivity (1.3 kOe) is relatively low but falls within the range reported for hematite (1−4 kOe). The much-higher value of M_s (0.42 emu/g) exhibited by the F2BT powder (47 wt % Fe_2O_3) annealed at 700 °C (see Figure 8d), which exceeds that of bulk Fe_2O_3, indicates the presence of a small amount of a second magnetic phase, most likely $BaFe_{12}O_{19}$. Considering its high saturation magnetization of 70 emu/g, even 2−3 wt % of barium hexaferrite (a quantity comparable to the XRD detection limit) can give a substantial contribution to the overall magnetization of the composite. The coercivity enhancement (from 1.3 kOe to 2.3 kOe and the slight deformation of the $M(H)$ loop also support the coexistence of two magnetic phases. The F1BT composites obtained by conventional sintering at 1050 and 1150 °C show constricted $M(H)$ loops characterized by a low coercivity (~0.1 kOe) at low fields, whereas at higher fields (> 0.2 kOe), the loops are open at both ends (see Figures 8b and 8c). On further rising the field, closing of the loops and magnetization saturation is observed. Similar constricted

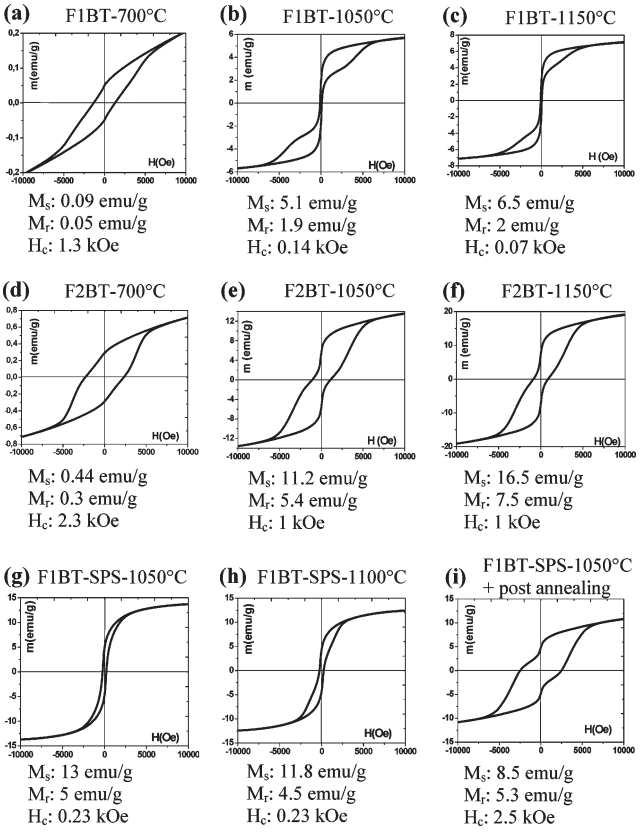

Figure 8. $M(H)$ hysteresis loops of composites obtained from Fe_2O_3@$BaTiO_3$ particles: (a) F1BT powder annealed at 700 °C, (b) F1BT sintered at 1050 °C, (c) F1BT sintered at 1150 °C, (d) F2BT powder calcined at 700 °C, (e) F2BT sintered at 1050 °C, (f) F2BT sintered at 1150 °C, (g) F1BT SPSed at 1050 °C, (h) F1BT SPSed at 1100 °C, and (i) F1BT SPSed at 1050 °C and post-annealead in air at 1000 °C.

(Perminvar-type) loops were reported for the Y-type hexagonal ferrite $Ba_2Co_{1.75}Zn_{0.25}Fe_{12}O_{22}$ and were related to a specific behavior of the domain walls and to anisotropy effects.[18] However, in the present case, the most likely origin of these constricted loops with "wasp-waisted" shape is the coexistence of two magnetic phases with widely different coercivities (soft and hard phases), as described in the case of natural and synthetic mixtures of magnetic oxides (in most cases, Fe_2O_3−Fe_3O_4 mixtures)[19−21] as well as in Nd−Fe−B and Co−Si−B permanent magnets.[22] Results reported in the literature also provide empirical confirmation that the total magnetization of the composite is the sum of the weighted contributions of each component, in the absence of significant magnetic interaction between particles.[19,21] Thus, to contribute significantly to the wasp-waisted behavior, a magnetic component must give rise to a significant portion

(18) Kojima, H. Fundamental Properties of Hexagonal Ferrites with Magnetoplumbite Structure. In *Ferromagnetic Materials*; Wohlfarth, E.P., Ed.; North-Holland: Amsterdam, 1987; Vol. *3*, pp 305−391.

(19) Roberts, A. P.; Cui, Y. L.; Verosub, K. L. *J. Geophys. Res.* **1995**, *100*, 17909.

(20) (a) Lees, J. A. *Geophys. J. Int.* **1997**, *131*, 335. (b) Hejda, P.; Kapička, A.; Petrovský, E.; Sjöberg, B. A. *IEE Trans. Magn.* **1994**, *30*, 881. (c) Jackson, M.; Worm, H.-U.; Banerjee, S. K. *Phys. Earth Planet. Inter.* **1990**, *65*, 78.

(21) Carvallo, C.; Muxworthy, A. R.; Dunlop, D. J. *Phys. Earth Planet. Inter.* **2006**, *154*, 308.

(22) (a) Heisz, S.; Hilscher, G. *J. Magn. Magn. Mater.* **1987**, *67*, 20. (b) Otani, Y.; Miyajima, H.; Chikazumi, S.; Hirosawa, S.; Sagawa, M. *J. Magn. Magn. Mater.* **1986**, *60*, 168. (c) Becker, J.-J. *IEEE Trans. Magn.* **1982**, *18*, 1451.

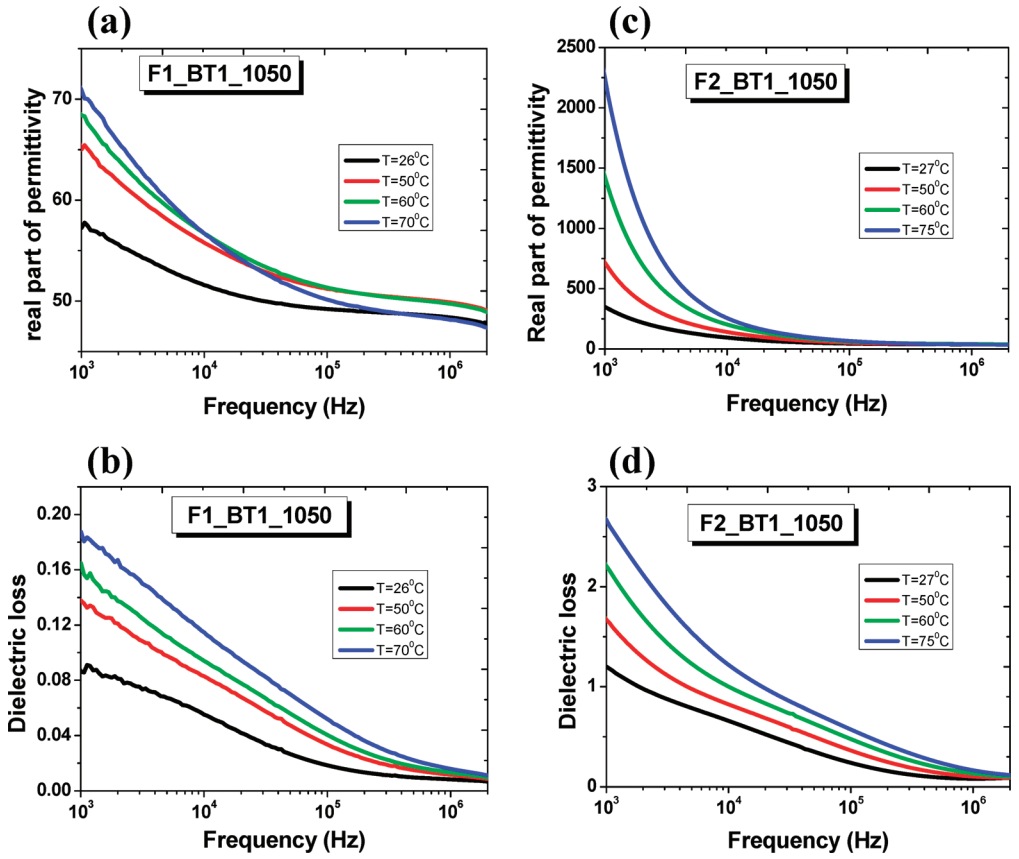

Figure 9. Dielectric properties of the F1BT and F2BT composites sintered at 1050 °C: (a) relative dielectric constant of F1BT, (b) dielectric losses in F1BT, (c) relative dielectric constant of F2BT, and (d) dielectric losses in F2BT.

of the total magnetization of the material. As a result, compounds with weak magnetic moments such as hematite must occur in large concentrations to cause constricted $M(H)$ loops in materials that also contain ferrimagnetic minerals. Therefore, according to the XRD results, the low-field behavior in Figures 8b and 8c should be controlled by the soft component, $Ba_{12}Fe_{28}Ti_{15}O_{84}$ (H_c = 0.04 kOe), while the high-field characteristics should be controlled by the hard component, $BaFe_{12}O_{19}$ (H_c = 4−6 kOe). The constriction of the $M(H)$ loops is expected to strongly reduce the maximum energy product of the material. The F2BT composites (see Figures 8e and 8f), prepared from powders containing a larger amount of Fe_2O_3, give hysteresis loops with higher coercivity (~1 kOe) and magnetization. The saturation magnetization (16.5 emu/g) of the material sintered at 1150 °C exceeds that of the quaternary ferrite (13 emu/g). These results indicate that the relative amount of the hard component, $BaFe_{12}O_{19}$, has significantly increased, in comparison to the F1BT composites, in agreement with the relative intensities of the XRD patterns (see Figure 4). The composites obtained by SPS (Figures 8g−i) display still different magnetic properties. In contrast to the samples obtained by conventional sintering, the XRD pattern (Figure 7) of the SPSed composites indicates the presence of Fe_3O_4. Accordingly, the coercivity of the sample obtained at 1050 °C (Figure 8g) is ~0.2 kOe and the magnetization is relatively high. However, the M_s value (13 emu/g) is much lower that the value (24 emu/g) expected by assuming complete reduction of Fe_2O_3 to Fe_3O_4, meaning that the transformation of hematite in magnetite has only occurred in the outer region of the sample. The slight opening of the $M(H)$ loop (see Figure 8g) supports this interpretation. Assuming a linear additivity, the percentage of Fe_3O_4 is estimated to be ~14.5 wt %. The presence of a harder magnetic phase is clearly observable from the $M(H)$ loop of the sample sintered at 1100 °C. While the coercivity is almost the same, the saturation magnetization has decreased to ~11.8 emu/g. The lower amount of magnetite can be explained by the shorter sintering time (3 min) at 1100 °C. Post-annealing in air at 800 and 1000 °C resulted in the formation of $BaFe_{12}O_{19}$ and $Ba_{12}Fe_{28}Ti_{15}O_{84}$ (see Figure 7) via the reaction of $BaTiO_3$ with Fe_3O_4/Fe_2O_3. The $M(H)$ loops (Figure 8i) are dominated by the hard component (the barium hexaferrite), and the coercivity increases to 2.5 kOe. In conclusion, composites with tunable magnetic properties resulting from the coexistence of hard and soft magnetic phases were obtained by controlling the solid-state reactions in Fe_2O_3@$BaTiO_3$ core−shell particles. This result was accomplished by varying the $Fe_2O_3/BaTiO_3$ volume ratio in the starting powder, the densification method, and the temperature of the post-annealing treatments. While the use of very small Fe_2O_3 particles must be avoided in the case of conventional sintering, because the reactions would be much faster and difficult to control, it could represent an additional opportunity to tailor the magnetic properties when densification occurs via SPS. Superparamagnetic behavior

is expected for small ferrimagnetic and ferromagnetic particles.

3.3. Dielectric Properties. The relative dielectric constant ε_r (the real part of the permittivity) of the F1BT composite sintered at 1050 °C is shown in Figure 9a. At high frequency (0.2−2 MHz), $\varepsilon_r \approx 50$ and increases with decreasing frequency up to 60−70 at 1 kHz. Such permittivity enhancement and the dispersion observed at lower frequency are common features of $BaTiO_3$-ferrite composites and indicates that some extrinsic phenomena, such as Maxwell−Wagner interfacial polarization and conductivity in the magnetic phases contribute to the permittivity.[6,23] The apparent permittivity of ferrites increases rapidly with decreasing frequency, because of conductivity effects. The relatively low dielectric constant of the composite (the dielectric constant of $BaTiO_3$ nanoceramics with a grain size of ∼100 nm is on the order of 1000)[24] must be ascribed to the rather high porosity of the composites. The tan δ measured in the range of 20−80 °C is ∼0.01 at 1 MHz and 0.08−0.16 at 1 kHz (see Figure 9b). These losses are significantly lower than those reported for most magnetoelectric $BaTiO_3$ and PZT composites[23,25] containing Ni or Co ferrite. Comparable low losses were reported for $MgFe_2O_4-BaTiO_3$ composites[26] and attributed to the intrinsic higher resistivity of the magnesium ferrite. The temperature dependence of the dielectric constant in the range of 20−80 °C is rather small: < 5% at 1 MHz. Sintering at higher temperature (1150 °C) determines and increase of both the dielectric constant (∼100 at 1 MHz, 200−350 at 1 kHz) and tan δ (between 0.05 and 0.4, depending on frequency and temperature). In any case, the relatively low dielectric losses indicate that percolation of the magnetic phases was avoided by the $BaTiO_3$ coating in composites containing 30 vol % Fe_2O_3, although the formation of a perovskite network reduced the final density. The F2BT composites display a lower permittivity at high frequency (∼40 at 1 MHz) and tan δ is ∼0.1 at 1 MHz and 1−2 at 1 kHz (see Figures 9c and 9d), in agreement with the extensive formation of the ferrimagnetic phases $BaFe_{12}O_{19}$ and $Ba_{12}Fe_{28}Ti_{15}O_{84}$, as indicated by XRD (recall Figure 4).

4. Summary and Conclusions

Multifunctional composites containing a dielectric/ferroelectric phase (tetragonal $BaTiO_3$) and two magnetic phases with contrasting coercivities (Fe_2O_3/Fe_3O_4, $BaFe_{12}O_{19}/Ba_{12}Fe_{28}Ti_{15}O_{84}$) were fabricated *in situ* by sintering $Fe_2O_3@BaTiO_3$ core−shell particles. The phase composition and, consequently, the magnetic properties of the composite materials can be controlled by varying the amount of Fe_2O_3 (30 or 50 vol %) in the starting powders, the densification technique (conventional or spark plasma sintering (SPS)) and the processing temperature. The reaction between Fe_2O_3 and $BaTiO_3$ in air proceeds at temperatures of ≥800 °C with the formation of barium hexaferrite ($BaFe_{12}O_{19}$) and the quaternary layered ferrite $Ba_{12}Fe_{28}Ti_{15}O_{84}$. However, the reaction kinetics is relatively slow and, even after 1 h sintering at 1150 °C, the system is not yet in chemical equilibrium, because it contains a significant fraction of tetragonal $BaTiO_3$ besides the two magnetic phases. In the case of composites processed via SPS, because of the very high heating rates (200 °C/min) and the short sintering time (3−4 min), the formation of new mixed phases is not detected by XRD after treatment at temperatures as high as 1050−1100 °C. Nevertheless, the local reducing conditions that exist in the SPS die determine the transformation of Fe_2O_3 to Fe_3O_4 in the outer region of the samples. Again, post-annealing treatments for 1 h at 800 and 1000 °C in air result in the formation of $BaFe_{12}O_{19}$ and $Ba_{12}Fe_{28}Ti_{15}O_{84}$. Notably, after annealing at 800 °C, Fe_2O_3 is not completely reacted and three magnetic phases coexist together. While the coercive field of Fe_3O_4 and $Ba_{12}Fe_{28}Ti_{15}O_{84}$ is in the range of 0.1−0.2 kOe (soft magnetic phases), the coercivity of Fe_2O_3 and $BaFe_{12}O_{19}$ is on the order of a few kOe (hard magnetic phases). As a result, the composites show constricted magnetic hysteresis loops originated by the coexistence of hard and soft magnetic oxides with widely different coercivities. The spontaneous magnetization of the composites is 5−16.5 emu/g, depending on the initial powder composition and processing conditions.

The use of $Fe_2O_3@BaTiO_3$ core−shell particles as precursors, in comparison to conventional $Fe_2O_3-BaTiO_3$ mixtures, has two main advantages. First, because the ferroelectric phase is far more insulating than the magnetic oxides, the coating of the Fe_2O_3 particles with a $BaTiO_3$ shell can prevent the percolation of the magnetic phase, resulting in lower dielectric losses, in comparison to composites obtained by conventional mixing. This effect was observed in the composites obtained from the powders initially containing 30 vol % Fe_2O_3, with losses between 1% and 10% at frequencies between 10 kHz and 1 MHz and temperatures of 20−80 °C. In contrast, the extensive formation of ferrites observed in the composites initially containing 50 vol % Fe_2O_3 leads to a significant increase of tan δ (0.1 at 1 MHz, 1−2 at 1 kHz). Second, because of the well-defined geometry of the core−shell particles, the formation of the new magnetic phases by reaction between $BaTiO_3$ and Fe_2O_3 can be better controlled and the final magnetic properties can be tailored by varying the processing conditions. Accordingly, it was not possible to reproduce the variety of hysteresis loops shown in Figure 8 by simply sintering $BaTiO_3-Fe_2O_3$ mixtures under the same experimental conditions.

(23) Yu, Z.; Ang, C. *J. Appl. Phys.* **2002**, *91*, 794.
(24) Zhao, Z.; Buscaglia, V.; Viviani, M.; Buscaglia, M. T.; Mitoseriu, L.; Testino, A.; Nygren, M.; Johnsson, M.; Nanni, P. *Phys. Rev. B* **2004**, *70*, 024107.
(25) (a) Patankar, K. K.; Dombale, P. D.; Mathe, V. L.; Patil, S. A.; Patil, R. N. *Mater. Sci. Eng., B* **2001**, *87*, 53. (b) Peng, T.-M.; Hsu, R.-T.; Jean, J.-H. *J. Am. Ceram. Soc.* **2006**, *89*, 2822. (c) Testino, A.; Mitoseriu, L.; Buscaglia, V.; Buscaglia, M. T.; Pallecchi, I.; Albuquerque, A. S.; Calzona, V.; Marrè, D.; Siri, A. S.; Nanni, P. *J. Eur. Ceram. Soc.* **2006**, *26*, 3031. (d) Harnagea, C.; Mitoseriu, L.; Buscaglia, V.; Pallecchi, I.; Nanni, P. *J. Eur. Ceram. Soc.* **2007**, *27*, 3947. (e) Jang, Q. H.; Shen, Z. J.; Zhou, J. P.; Shi, Z.; Nan, C.-W. *J. Eur. Ceram. Soc.* **2007**, *27*, 279. (f) Huang, J.; Du, P.; Hong, L.; Dong, Y.; Hong, M. *Adv. Mater.* **2007**, *19*, 437. (g) Zhang, L.; Zhai, J.; Mo, W; Yao, X. *Mater. Chem. Phys.* **2009**, *118*, 208.
(26) Tan, S. Y.; Shannigrahi, S. R.; Tan, S. H.; Tay, F. E. H. *J. Appl. Phys.* **2008**, *103*, 094105.

Our results provide evidence of the possibility of fabricating multifunctional composites by *in situ* solid-state reactions using suitable reactive precursors. More generally, reactive precursors and templates represent useful tools for the fabrication of a variety of nanostructured materials, such as nanowires, nanotubes, hollow particles, and ceramics with locally graded composition.[14,15c,27] Well-designed reactive templates allow for a careful control of the solid-state reaction at the nanoscale, thus enabling the fabrication of materials and composites with specific morphologies, microstructure/nanostructure, and functional properties. Therefore, material synthesis can be implemented as a knowledge-driven procedure rather than a trial-and-error process.

Acknowledgment. The financial support from the Romanian Ministry of Education, Research and Innovation (CNCSIS-PCCEID-76 grant) is acknowledged.

(27) (a) Fan, H. J.; Knez, M.; Scholz, R.; Nielsch, K.; Pippel, E.; Hesse, D.; Zacharias, M.; Gösele, U. *Nat. Mater.* **2006**, *5*, 627. (b) Buscaglia, M. T.; Buscaglia, V.; Viviani, M.; Dondero, G.; Röhrig, S.; Rüdiger, A.; Nanni, P. *Nanotechnology* **2008**, *19*, 225602. (c) Buscaglia, M. T.; Viviani, M.; Zhao, Z.; Buscaglia, V.; Nanni, P. *Chem. Mater.* **2006**, *18*, 4002.